Eur. J. Mineral.
2018, **30**, 289–304
Published online 4 May 2018

Special issue – Mineral Diversity, Complexity and Evolution

Betalomonosovite: chemical and structural variability and genesis

INNA S. LYKOVA[1,2,*], NIKITA V. CHUKANOV[3], IGOR V. PEKOV[2], VASILIY O. YAPASKURT[2] and GERALD GIESTER[4]

[1] Fersman Mineralogical Museum RAS, Leninsky Prospekt 18-2, 119071 Moscow, Russia
*Corresponding author, e-mail: innalykova@mail.ru
[2] Faculty of Geology, Moscow State University, Vorobievy Gory, 119991 Moscow, Russia
[3] Institute of Problems of Chemical Physics RAS, Chernogolovka, Moscow Region 142432, Russia
[4] Institute of Mineralogy and Crystallography, University of Vienna, Althanstrasse 14, 1090 Vienna, Austria

Abstract: The crystal structures of four betalomonosovite samples from peralkaline pegmatites of the Khibiny alkaline complex, Kola Peninsula, Russia, were studied using single-crystal X-ray diffraction. The samples represent different chemical and structural varieties of betalomonosovite. The suggested general formula of betalomonosovite, based on the empirical data known to date, is $Na_{5+x}Ti_4[Si_2O_7]_2[PO_3(OH)]_{2-y}[PO_2(OH)_2]_yO_2[(OH,F)_{2-z}O_z]$, where $0 \le x \le 2$, $0 \le y \le 1$ and $0 \le z \le 1$. Betalomonosovite is a transformation product of lomonosovite, $Na_{10}Ti_4(Si_2O_7)_2(PO_4)_2O_4$, due to the leaching of Na and protonation of O atoms of phosphate groups and Ti–O–Ti bridges. Distinctive features of betalomonosovite are: (a) the presence of H^+ in the form of species-defining acid phosphate anion(s) $[PO_2(OH)_2] \pm [PO_3(OH)]$; (b) the presence of OH^- anion at the Ti–O–Ti bridges in the *O* sheet of the *HOH* block and c) deficiency of Na (as compared to lomonosovite) in an amount related to the degree of protonation. A hypothetical end-member product of lomonosovite alteration with the simplified formula $Na_4Ti_4[Si_2O_7]_2[PO_2(OH)_2]_2O_2(OH)_2$ has not been reported in Nature yet. The ways and the degree of alteration may vary significantly, resulting in significant variations in both crystal structure and chemical composition, including the Na content, the degree of the substitution of O by OH, unit-cell dimensions and splitting of the P, O and/or Na sites.

Key-words: betalomonosovite; lomonosovite; heterophyllosilicate; transformation mineral; titanosilicate; crystal structure; peralkaline rock; Khibiny alkaline complex; Kola Peninsula.

1. Introduction

Betalomonosovite is a layered sodium titanosilicate with additional sodium cations and hydrophosphate anions intercalated between titanosilicate layers. It is considered as a heterophyllosilicate belonging to the bafertisite mero-plesiotype series by Ferraris & Gula (2005) or a TS-block mineral by Sokolova (2006). It was described as a new mineral by Gerasimovskiy & Kazakova (1962) from the Lovozero alkaline complex, Kola Peninsula, Russia, and named in allusion to its close relation to the H-free species lomonosovite, $Na_{10}Ti_4(Si_2O_7)_2(PO_4)_2O_4$. The above-cited paper was published without formal approval of the mineral by the IMA Commission on New Minerals and Mineral Names and betalomonosovite was not considered as a valid mineral species until recently.

Betalomonosovite is a typical accessory mineral of some peralkaline (hyperagpaitic) rocks and pegmatites in the Khibiny alkaline complex. It is less common in Lovozero and was recently found in the Kovdor alkaline-ultrabasic complex (Kola Peninsula, Russia; see Khomyakov, 1995; Ageeva, 1999; Pekov, 2000; Moiseev & Chukanov, 2007). Ageeva (1999) distinguished two genetic varieties of betalomonosovite in Khibiny: (1) a product of post-crystallization metasomatic alteration of lomonosovite in pyroxene rischorrites and (2) a primary accessory mineral in pegmatites. Chemical and morphological signs of the secondary nature of betalomonosovite in rischorrites are given in the cited paper, while the primary nature of the mineral in pegmatites is less well ascertained.

There have been multiple reports on the crystal structure of betalomonosovite (Rastsvetaeva *et al.* 1975; Rastsvetaeva, 1986, 1988, 1989; Khalilov, 1990), but with little agreement between them, even in the unit-cell dimensions. This fact, as well as the difficulties in obtaining reliable and consistent results on its chemical composition resulted in a doubtful status of betalomonosovite as mineral species. After the recent reappraisals of the crystal structure and chemistry of betalomonosovite (Yakubovich *et al.* 2014; Borutzky *et al.* 2014; Sokolova *et al.* 2015a), the IMA Commission on New Minerals, Nomenclature and Classification (CNMNC) approved betalomonosovite as a valid mineral species with the idealized formula $Na_6\square_4Ti_4(Si_2O_7)_2[PO_3(OH)][PO_2(OH)_2]O_2(OF)$ based on proposal 14-J submitted by Sokolova *et al.* (2015b).

However, recent structural studies (Yakubovich *et al.* 2014; Sokolova *et al.* 2015a) demonstrated the same discrepancies as reported previously without providing much explanation. The aim of the present study is therefore:

https://doi.org/10.1127/ejm/2018/0030-2719
0935-1221/18/0030-2719 $ 7.20

(1) to clarify the ambiguity in the interpretation of the crystal structure of betalomonosovite, (2) to define its variability in both chemical and structural aspects and (3) to determine possible mechanisms of its formation in Nature.

2. Previous work

Gerasimovskiy & Kazakova (1962) demonstrated the similarity of betalomonosovite and lomonosovite in terms of their chemistry, X-ray diffraction data and physical properties. Sokolova *et al.* (1971) defined the main difference between these minerals as a partial substitution of O^{2-} in PO_4 tetrahedra in lomonosovite by OH^- in betalomonosovite, associated with formation of acid phosphate groups.

The first structural model of betalomonosovite (Rastsvetaeva *et al.* 1975) confirmed the similarity of these species. Their structures are based upon the same heterophyllosilicate *HOH* block. The central octahedral *O* sheet is composed by close-packed Na- and Ti-centered polyhedra and sandwiched between two identical heteropolyhedral *H* sheets consisting of alternating $[Si_2O_7]$ groups and Ti- and Na-centered polyhedra. The unit cell of betalomonosovite was characterized by a doubled *b* parameter (14.3 Å) as compared to lomonosovite (7.1 Å), and the contents of their interlayer space were reported as different (Table 1; Belov *et al.* 1977, Cámara *et al.* 2008). There are seven fully occupied Na sites and two P sites per unit cell in betalomonosovite. Two vertices in one of the P-centered tetrahedra [site P2] were reported to be occupied by OH groups, while the other tetrahedron [centered by P1] had only one OH group. Thus the presence of both $[PO_3(OH)]$ and $[PO_2(OH)_2]$ groups was considered. The structure was solved based on data collected by the X-ray photographic technique with a relatively high *R* value of 15.4% (Rastsvetaeva *et al.* 1975).

Another model of betalomonosovite structure was also described based on the unit cell with a doubled *b* parameter (Table 1, Rastsvetaeva, 1986). This study reported ten Na sites with the occupancies ranging from 20 to 85%, resulting in approximately five alkali metal cations per formula unit (*pfu*). One of the P sites was split into two subsites with the occupancies of 60 and 20%, and the presence of only doubly protonated phosphate groups $[PO_2(OH)_2]$ was reported (Rastsvetaeva, 1986).

A new model of betalomonosovite structure, with the "small", lomonosovite-type unit cell and the space group $P1$ (Table 1), was reported by Rastsvetaeva (1988). The study revealed ten partially occupied Na sites (with occupancies of 22–81%) and both P sites were reported as split: one into two subsites, the other into three subsites. However, the short (1.20–1.32 Å) P–O distances of three PO_4 tetrahedra casted doubts about the validity of the model. Again, the presence of only doubly protonated phosphate groups was reported (Rastsvetaeva, 1988).

Based on the cited works, Rastsvetaeva (1989) assumed a domain structure for betalomonosovite. According to this model, unit cells with different dimensions (Rastsvetaeva *et al.* 1975; Rastsvetaeva, 1986, 1988) segregate into domains, replacing each other in one direction; one crystal may contain different domains in various proportions. The obtained models were considered to be ordered ("monodomain"; Rastsvetaeva *et al.* 1975), partially ordered (Rastsvetaeva, 1986), and disordered ("polydomain"; Rastsvetaeva, 1988).

Khalilov (1990) obtained a model based on the same single-crystal X-ray diffraction data set as Rastsvetaeva (1988) and refined it in both $P1$ and $P\bar{1}$ space groups (Table 1). There were four reported fully and six partially occupied (with occupancies of 22–81%) Na sites in the acentric model and two fully and three partially occupied (with occupancies of 31–81%) Na sites in the centrosymmetric model. Splitting of the P sites was not observed and both P-centered tetrahedra were described as $[PO_2(OH)_2]$ (Khalilov, 1990).

Yakubovich *et al.* (2014) suggested a model based on the "small", lomonosovite-type unit cell and the space group $P\bar{1}$. There were one fully and four partially occupied Na sites with the total of approximately five large cations *pfu*. The P site was reported as split into the two half-occupied subsites; the presence of only doubly protonated phosphate groups was reported (Table 1).

The latest of the published models (Sokolova *et al.* 2015a), as in the early works, was characterized by the doubled *b* parameter as compared to lomonosovite (Table 1; Rastsvetaeva *et al.* 1975; Rastsvetaeva, 1986). There were ten partially occupied Na sites and two P sites, both split into two subsites with 86 and 14% occupancies. The presence of both $[PO_3(OH)]$ and $[PO_2(OH)_2]$ groups was reported. The model presented by Sokolova *et al.* (2015a) is similar to that reported by Rastsvetaeva *et al.* (1975).

Thus, the six above mentioned structural reports on betalomonosovite differ from each other in several aspects, including unit-cell dimensions, numbers and occupancies of the large-cation sites, splitting of the P sites and the presence or absence of $[PO_3(OH)]$ groups. We suggest these discrepancies cannot be explained by the refinement errors but rather result from significant chemical and structural variations of the mineral.

3. Samples

Four samples of betalomonosovite from different pegmatite bodies within the Khibiny alkaline complex, Kola Peninsula, Russia, were selected for this study on the basis of distinct differences in their IR spectra:

– *Sample ST4992* is from the Apatitovyi Tsirk (Apatite Cirque) open pit of the Rasvumchorr apatite mine at Mt. Rasvumchorr. This specimen is from the V.I. Stepanov collection now deposited in the Fersman Mineralogical Museum of the Russian Academy of Sciences, Moscow. Betalomonosovite forms yellow lamellar crystals (2.0–3.5 cm in size) associated with hydrodelhayelite, eudialyte and lamprophyllite in rischorritic pegmatite;

Table 1. Unit-cell parameters and composition of the main structural units for betalomonosovite and lomonosovite (Lom).

Mineral	*a*, Å	*b*, Å	*c*, Å	α, °	β, °	γ, °	*V*, Å^3	*HOH* block	Interlayer space	R^{***}, %	References
Lom	5.41–5.49	7.11–7.12	14.48–14.50	100–101	96–97	90	546–552	$Na_4Ti_4[Si_2O_7]_2O_4$*	$Na_6(PO_4)_2$*	–	Belov *et al.*, 1977; Cámara *et al.*, 2008; Lykova *et al.*, 2015
Betalomonosovite	5.34	14.26	14.23	102.5	105.9	89.1	1016	$Na_4Ti_4[Si_2O_7]_2O_4$*	$Na_3[PO_3(OH)][PO_2(OH)_2]$*	15.4	Rastsvetaeva *et al.*, 1975
	5.33	14.18	14.47	102.2	95.5	90.2	1063	$(Na_{2.3}Ca_{0.1}K_{0.2})(Ti_{3.03}Nb_{0.3}Zr_{0.157}Fe^{3+}_{0.3}Mn_{0.2}Mg_{0.05})[Si_2O_7]_2O_4$	$[Na_{2.6}(H_2PO_4)_2]$**	8.7	Rastsvetaeva, 1986
	5.35	7.13	14.49	102.1	95.2	90.2	538	$Na_{1.50}(Ti_{2.8}Fe^{3+}_{0.65}Nb_{0.4}Mn_{0.15})[Si_2O_7]_2O_4$	$(Na_{3.05}Ca_{0.5})[PO_2(OH)_2]_2$**	4.8	Rastsvetaeva, 1988
	5.35	7.13	14.49	102.1	95.2	90.2	538	$Na_4Ti_4[Si_2O_7]_2O_2(OH,F)_2$*	$Na_2[PO_2(OH)_2]_2$*, **	5.5	Khalilov, 1990
	5.32	7.09	14.45	102.9	96.4	90.3	527	$(Na_{1.42}Ca_{0.71})(Ti_{3.63}Nb_{0.03}Fe^{3+}_{0.34})[Si_2O_7]_2(O, OH, F)_4$*	$Na_{3.00}Mn^{2+}_{0.11}[H_2PO_4]_2$**	5.7	Yakubovich *et al.*, 2014
	5.33	14.17	14.51	103.2	96.3	90.3	1061	$Na_4Ti_4[Si_2O_7]_2O_2(OF)$*	$Na_2[PO_3(OH)][PO_2(OH)_2]$*	6.4	Sokolova *et al.*, 2015a
	5.34	14.12	14.43	100.8	96.0	90.0	1062	$Na_3Ti_4[Si_2O_7]_2O_3(OH)$*	$Na_4[PO_3(OH)]_2$*	4.3	This work, ST4992
	5.34	7.10	14.37	101.1	95.4	89.8	532	$Na_2Ti_4[Si_2O_7]_2O_2(OH)_2$*	$Na_4[PO_3(OH)]_2$*	4.9	This work, Ko0151
	5.32	14.13	14.41	101.9	96.0	90.1	1054	$Na_2Ti_4[Si_2O_7]_2O_2(OH)_2$*	$Na_4[PO_3(OH)]_2$	8.4	This work, GIM6019
	5.30	14.15	14.44	103.4	96.5	90.4	1046	$Na_2Ti_4[Si_2O_7]_2O_2(OH)_2$	$Na_3[PO_3(OH)][PO_2(OH)_2]$*	9.6	This work, OlR0194

* Idealized formula.
** The correctness of the including of only doubly protonated phosphate groups H_2PO_4 in formula is discussed in details in text, the section Discussion.
*** For betalomonosovite.

Fig. 1. Partial pseudomorphs of betalomonosovite (1) after tabular crystals of lomonosovite (2); sample Rsv0259_0260 *in situ*. Apatitovyi Tsirk, Mt. Rasvumchorr, Khibiny alkaline complex, Kola Peninsula, Russia. Field of view: 11 cm.

– *Sample Ko0151* is from the outer zone of the Shcherbakovitovoe pegmatite, Koashva open pit belonging to the Vostochnyi (Eastern) apatite mine and located at Mt. Koashva. Betalomonosovite occurs as yellow lamellar crystals up to 2 cm in size partially replaced by murmanite and calciomurmanite (Lykova *et al.* 2016) and associated with microcline, aegirine, nepheline, sodalite, lamprophyllite and eudialyte;
– *Sample GIM6019* is from the Vostochnyi apatite mine originates from the collections of the Bel'kov Museum of Geology and Mineralogy of the Geological Institute of Kola Science Center, Russian Academy of Sciences, Apatity. Betalomonosovite forms yellow tabular crystals up to 2 × 5 cm in size associated with lamprophyllite, pectolite, aegirine and eudialyte;
– *Sample OlR0194* is from the Olenii Ruchei (Reindeer Creek) open pit (level + 375 m) of the Olenii Ruchei apatite mine at Mt. Niorkpakhk. Betalomonosovite occurs as beige lamellar crystals up to 4 cm in size with microcline, aegirine and lamprophyllite.

In 2015, partial pseudomorphs of betalomonosovite after lomonosovite (*sample Rsv0260_0259*) were found by the authors (IVP and ISL) in the Apatitovyi Tsirk. Dark-brown tabular crystals of lomonosovite up to 1 cm in size are partially replaced by beige betalomonosovite (Fig. 1).

4. Experimental procedure

The chemical composition of betalomonosovite (Table 2) was studied in the Laboratory of local methods of matter investigation (Faculty of Geology, Moscow State University) with a Jeol JSM-6480LV scanning electron microscope equipped with energy-dispersive spectrometer (EDS) INCA Energy 350 under the following conditions: operating voltage 20 kV, beam current 6.5 nA and electron beam diameter 2 μm. The standards used were: lorenzenite (Na*K*α, Si*K*α, Ti*K*α), diopside (Mg*K*α), wollastonite

Table 2. Chemical composition of the studied betalomonosovite samples.

	ST4992		Ko0151		GIM6019		OlR0194	
wt.%								
Na_2O	21.22	20.62	17.22	19.10	17.41	18.08	15.32	14.22
K_2O	0.13	0.11	–	–	–	–	0.08	–
CaO	2.53	2.49	2.34	2.38	3.03	2.91	3.13	3.16
MgO	0.24	0.26	0.63	0.77	0.42	0.47	0.53	0.51
MnO	0.31	0.36	2.00	1.96	0.73	0.67	0.80	0.79
Fe_2O_3	2.86	2.93	2.47	2.36	3.60	3.58	3.51	3.52
Al_2O_3	–	–	0.22	–	–	–	0.12	0.14
SiO_2	25.30	24.44	23.01	25.24	25.70	25.22	26.03	25.74
TiO_2	27.23	27.30	22.67	24.11	27.33	27.11	27.21	27.12
Nb_2O_5	0.57	0.50	4.25	4.72	0.91	0.97	1.57	1.52
P_2O_5	14.97	14.64	13.26	14.65	14.89	14.82	15.17	14.67
F	–	–	0.41	0.64	–	–	–	–
$-O=F_2$			0.17	0.27				
Total	95.36	93.65	88.31	95.66	94.02	93.83	93.47	91.39
Atoms per formula unit (based on Si + Al = 4)								
Na	6.50	6.54	5.75	5.87	5.25	5.56	4.54	4.26
K	0.03	0.02	–	–	–	–	0.02	–
Ca	0.43	0.44	0.43	0.41	0.50	0.49	0.51	0.52
Mg	0.06	0.07	0.16	0.18	0.10	0.11	0.12	0.12
Fe	0.34	0.36	0.32	0.28	0.42	0.43	0.40	0.41
Mn	0.04	0.05	0.29	0.26	0.10	0.09	0.10	0.10
Al	–	–	0.04	–	–	–	0.02	0.03
Si	4.00	4.00	3.96	4.00	4.00	4.00	3.98	3.97
Ti	3.24	3.36	2.95	2.87	3.20	3.23	3.13	3.15
Nb	0.04	0.04	0.33	0.34	0.06	0.07	0.11	0.11
P	2.00	2.03	1.93	1.97	1.96	1.99	1.96	1.92
F	–	–	0.23	0.32	–	–	–	–

ST4992–Apatitovyi Tsirk, Mt. Rasvumchorr; *Ko0151*–Shcherbakovitovyi pegmatite, Koashva open pit, Mt. Koashva; *GIM6019*–Vostochnyi mine; *OlR0194*–Olenii Ruchei open pit, Mt. Niorkpakhk (all – Khibiny alkaline complex, Kola peninsula, Russia). Dash means the content of a constituent below detection limit.

(Ca*K*α), sanidine (K*K*α), hornblende (Al*K*α), GaP (P*K*α), Nb (Nb*L*α), Mn (Mn*K*α), orthopyroxene (Fe*K*α) and MgF_2 (F*K*α). Iron and manganese oxidation states and H_2O content were not determined directly.

Infrared (IR) absorption spectra were obtained from powdered samples mixed with dried KBr, pelletized, and analyzed using a Bruker Optics ALPHA FTIR spectrometer in the wave number range 360 to 3800 cm^{-1}, with a resolution of 4 cm^{-1} and 16 scans accumulated. The IR spectrum of an analogous pellet of pure KBr was used as a reference.

Crystal-structure studies were carried out using single-crystal diffraction data collected in a full sphere of the reciprocal space on a Bruker Kappa X8 APEX diffractometer equipped with a CCD detector at $T = 200$ K. The measured intensities were corrected for Lorentz, background, polarization and absorption effects. All crystal structures reported here were solved by direct methods and refined by full-matrix least-squares techniques on F^2 in the space group $P\bar{1}$ using the SHELX-97 program package (Sheldrick, 2008). The crystal data, the details of the X-ray diffraction experiments and the structure refinement parameters are given in Table 3.

The crystal structures of samples ST4992, Ko0151, GIM6019 and OlR0194 were refined to *R* values of 4.32, 4.96, 8.41 and 9.55% on the basis of 4714, 2401, 4829 and 4171 unique reflections with $I > 2\sigma(I)$, respectively. Sample Ko0151 was described in the lomonosovite-type unit cell, while three other samples have shown additional reflections in the reciprocal space along the **b*** axis, which indicated the presence of the doubled *b* parameter as compared to lomonosovite (Table 1).

5. Results

5.1. Chemical composition

The betalomonosovite crystal fragments used for the crystal-structure studies were analysed. The chemical data are given in Table 2, showing that the main variations are in Na contents and analytical totals. Low or nil fluorine contents are a consistent feature. The averaged (based on the analyses given in Table 2) empirical formulae calculated on the basis of Si + Al = 4 *apfu* (with the OH^-/O^{2-} ratio calculated by charge balance, assuming a trivalent state of Fe) are:

ST4992,

$$(Na_{6.52}Ca_{0.43}K_{0.02})_{\Sigma 6.97}(Ti_{3.30}Fe^{3+}_{0.35}Mg_{0.06}Nb_{0.04}Mn_{0.04})_{\Sigma 3.79}Si_{4.00}P_{2.02}O_{22.15}(OH)_{3.85};$$

Table 3. Crystal data, data-collection information and structure-refinement details for betalomonosovite.

Sample	ST4992	Ko0151	GIM6019	OlR0194
Space group, Z	$P\bar{1}$, 1	$P\bar{1}$, 1	$P\bar{1}$, 1	$P\bar{1}$, 1
a, Å	5.33724(15)	5.33733(19)	5.3185(3)	5.30090(18)
b, Å	14.1183(4)	7.1044(3)	14.1333(9)	14.1460(4)
c, Å	14.4274(4)	14.3719(5)	14.4147(8)	14.4435(4)
α, °	100.8291(14)	101.053(2)	101.934(3)	103.3862(15)
β, °	96.0276(14)	95.447(2)	96.040(3)	96.5126(16)
γ, °	90.0308(15)	89.831(3)	90.120(3)	90.4128(17)
V, Å^3	1061.65(5)	532.37(3)	1053.89(10)	1046.21(6)
λ (Mo*K*α) (Å), *T* (K)	0.71073, 200(2)			
Diffractometer	Kappa X8 APEX CCD			
Reflections collected	31095	13287	29985	31751
Number of unique reflections, R_{int}	5236, 0.0278	2631, 0.0390	5174, 0.0311	5143, 0.0420
Reflections with $I > 2\sigma(I)$	4714	2401	4829	4171
Refinement on	F^2			
Number of refined parameters	465	231	461	401
R_1	0.0432	0.0496	0.0841	0.0955
w$R_{2all}(F^2)$	0.0988	0.0999	0.1655	0.1792
GoF	1.013	1.099	1.126	1.126
$\Delta\rho_{max}$ /$\Delta\rho_{min}$ (e/Å^3)	1.024/−1.007	0.796/−0.785	1.113/−1.041	1.851/−1.270

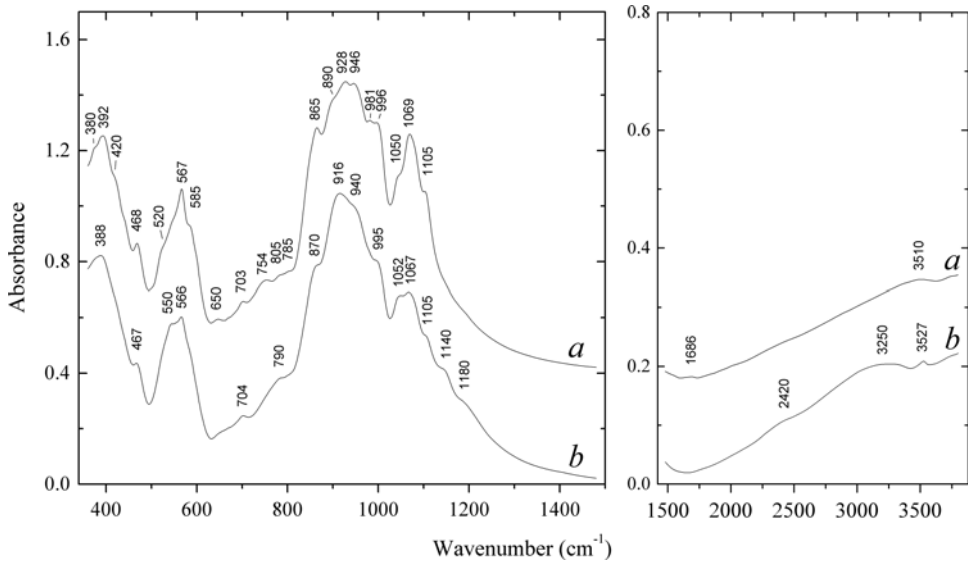

Fig. 2. IR spectra of lomonosovite (a) and betalomonosovite (b) in sample Rsv0259_0260. The spectra are offset for comparison.

Ko0151,
$(Na_{5.81}Ca_{0.42})_{\Sigma 6.23}(Ti_{2.91}Nb_{0.33}Fe^{3+}_{0.30}Mn_{0.28}Mg_{0.17})_{\Sigma 3.99}(Si_{3.98}Al_{0.02})_{\Sigma 4.00}P_{1.95}O_{21.47}(OH)_{4.26}F_{0.27}$;

GIM6019,
$(Na_{5.40}Ca_{0.50})_{\Sigma 5.90}(Ti_{3.22}Fe^{3+}_{0.43}Mg_{0.10}Mn_{0.09}Nb_{0.07})_{\Sigma 3.91}Si_{4.00}P_{1.97}O_{21.15}(OH)_{4.85}$;

OlR0194,
$(Na_{4.40}Ca_{0.52}K_{0.01})_{\Sigma 4.93}(Ti_{3.14}Fe^{3+}_{0.41}Mg_{0.12}Nb_{0.11}Mn_{0.10})_{\Sigma 3.88}(Si_{3.98}Al_{0.02})_{\Sigma 4.00}P_{1.94}O_{19.91}(OH)_{6.06}$.

5.2. Infrared spectroscopy

The IR spectrum of lomonosovite from sample Rsv0260_0259 (Fig. 2a) is close to that of unaltered lomonosovite (Chukanov, 2014), but is characterized by a worse band resolution and the presence of weak bands of O–H-stretching vibrations and bending vibrations of H_2O molecules (at 3510 and 1686 cm^{-1}, respectively). Acid OH groups are absent. The bands in the ranges 1050–1105, 865–996, 650–785, 520–585 and below 500 cm^{-1} correspond to asymmetric P–O stretching vibrations of PO_4^{3-}anions [$\nu_3(F_2)$ mode], Si–O–stretching, O–Si–O

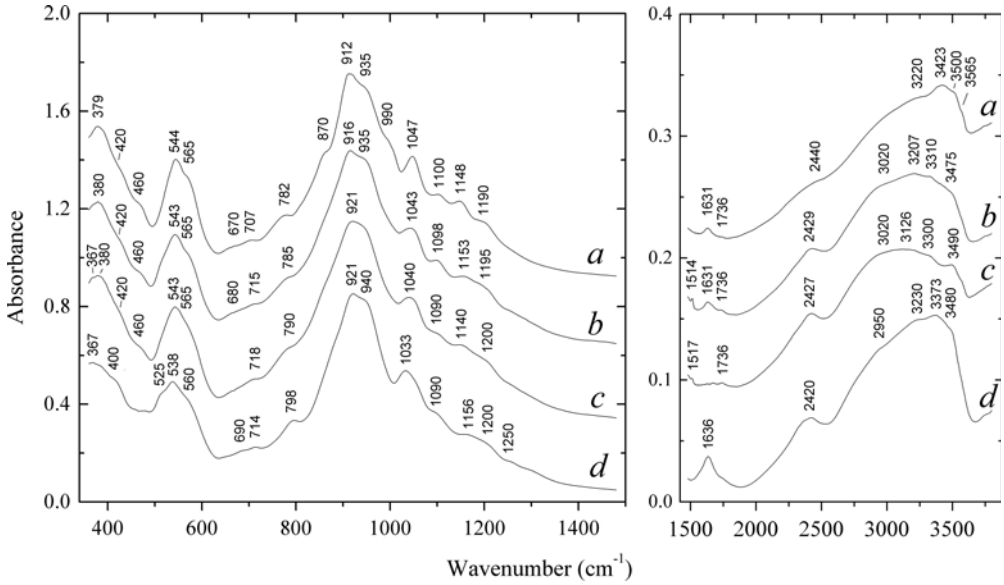

Fig. 3. IR spectra of betalomonosovite: samples ST4992 (a), Ko0151 (b), GIM6019 (c) and O1R0194 (d). The spectra are offset for comparison.

bending, O–P–O bending [$\nu_4(F_2)$ mode, partly mixed with Ti–O-stretching] vibrations and mixed lattice modes involving Si–O–Si bending and ν_2(E) O–P–O bending vibrations, respectively.

The IR spectra of all betalomonosovite samples (Fig. 2b, Fig. 3a–c) contain bands of acid phosphate groups in the ranges 2400–3300 cm^{-1} (O–H-stretching vibrations) and 1140–1250 cm^{-1} (P–O-stretching modes). The degree of protonation increases in the sequence: Rsv0260_0259 < ST4992 < Ko0151 ≈ GIM6019 < O1R0194. The samples ST4992 and Ko0151 contain minor amounts of H_2O molecules absorbing at 1631 and 3300–3400 cm^{-1}, whereas samples Rsv0260_0259 and GIM6019 are practically H_2O-free. Sample O1R0194 is the most hydrated. Relatively narrow bands and shoulders in the range 3475–3527 cm^{-1} correspond to basic OH groups (OH^- anions). Very weak bands at 1514–1517 and 1736 cm^{-1} are tentatively assigned to the vibrations of H^+ cation coordinated by O atoms and hydronium cations (or its hydrated analogue Zundel cation, $H_5O_2^+$), respectively. The assignment of absorption bands was made in accordance with Nakamoto (2008, 2009) and Chukanov & Chervonnyi (2016).

Absorptions in the ranges 2950–3150 and 3200–3300 cm^{-1} can be assigned to stretching vibrations of the covalent O–H bonds with *H* atoms forming medium-strength hydrogen bonds. The bands in the range 2420–2440 cm^{-1} correspond to acid groups forming strong hydrogen bonds with the O···O distances of 2.58 ± 0.02 Å (Libowitzky, 1999).

5.3. Single-crystal X-ray diffraction studies

All four structures refined in this work contain the same *HOH* block. Cation sites in the structure of Ko0151 were labeled according to the nomenclature introduced by Belov *et al.* (1977) [and later adopted by Cámara *et al.* (2008)], while in the structures with the *b*-doubled unit cell, double labels were assigned that correspond to the sites in lomonosovite with 'a' and 'b' letters used for the sites related by the *b*/2 translation. For example, Ti sites in the *H* sheet are labeled as Ti(1) in lomonosovite and in sample Ko0151, and as Ti(1a) and Ti(1b) in betalomonosovite samples with doubled *b* parameter. Atom coordinates, equivalent displacement parameters, site occupancy factors or refined site-scatterings, bond-valence sums (Brese & O'Keeffe, 1991) and selected interatomic distances for all four samples are given in Tables 4–7 and Tables S1–S8, freely available as Supplementary Material linked to this article on the GSW website of the journal.

Detailed description of the *HOH* block and interlayer space content in betalomonosovite can be found in works cited in the "Previous work" section. Figure 4 shows a general view of the crystal structure of sample ST4992 as an example. Here we would like to focus on large-cation and phosphorus sites as they are (a) essentially different from structure to structure and (b) crucial for the definition of betalomonosovite as a mineral species and the determination of its origin.

5.3.1. Sample ST4992

There are ten large-cation sites in the crystal structure of this sample. In the interlayer space, Na(3a) and Na(3b) sites are predominantly occupied (98 and 86%, respectively) while the adjacent Na(4a) and Na(4b) are mainly vacant with occupancies of 44 and 40%. Occupancies of other six sites fall in the interval between these values resulting in approximately 7 large cations *pfu*. Translationally pseudo-equivalent sites generally have roughly similar occupancies with the notable exception of Na(5a) and Na(5b), where the Na(5b) site is split into two subsites

Table 4. Selected interatomic distances (Å) for betalomonosovite sample ST4992.

P(1a)–O(24)	1.510(4)	Na(1b)–O(25)	2.294(6)	Na(3a)–O(26)	2.220(5)	Na(4b)–O(21)	2.191(11)
P(1a)–O(19)	1.518(3)	Na(1b)–O(10)	2.368(4)	Na(3a)–O(27)	2.22(3)	Na(4b)–O(23)	2.218(7)
P(1a)–O(23)	1.532(5)	Na(1b)–O(12)	2.434(3)	Na(3a)–O(28)	2.22(5)	Na(4b)–O(27)	2.30(4)
P(1a)–O(26)	1.547(4)	Na(1b)–O(6)	2.453(3)	Na(3a)–O(23)	2.385(7)	Na(4b)–O(6)	2.327(5)
⟨P(1a)–O⟩	1.527	Na(1b)–O(17)	2.576(3)	Na(3a)–O(8)	2.434(3)	Na(4b)–O(21′)	2.51(2)
		Na(1b)–O(8)	2.757(3)	Na(3a)–O(19)	2.448(4)	Na(4b)–O(25)	2.566(9)
P(1a′)–O(27)	1.489(18)	Na(1b)–O(4)	2.847(4)	Na(3a)–O(12)	2.547(3)	Na(4b)–O(25)	2.831(9)
P(1a′)–O(19)	1.512(17)	⟨Na(1b)–O⟩	2.533	Na(3a)–O(9)	2.649(3)	⟨Na(4b)–O⟩	2.43/2.49/2.44/2.51[5]
P(1a′)–O(28)	1.55(5)			⟨Na(3a)–O⟩	2.447/2.42[2]		
P(1a′)–O(24)	1.556(14)	Na(2a)–O(1)	2.244(3)			Na(5a)–O(26)	2.285(5)
⟨P(1a′)–O⟩	1.53	Na(2a)–O(16)	2.374(3)	Na(3b)–O(21)	2.069(10)	Na(5a)–O(25)	2.332(5)
		Na(2a)–O(1)	2.394(3)	Na(3b)–O(22)	2.267(5)	Na(5a)–O(19)	2.404(4)
P(1b)–O(22)	1.489(4)	Na(2a)–O(18)	2.420(3)	Na(3b)–O(21″)	2.386(9)	Na(5a)–O(23)	2.418(6)
P(1b)–O(25)	1.499(4)	Na(2a)–O(16)	2.608(3)	Na(3b)–O(11)	2.419(3)	Na(5a)–O(12)	2.603(4)
P(1b)–O(20)	1.525(3)	Na(2a)–O(14)	2.723(3)	Na(3b)–O(20)	2.506(4)	Na(5a)–O(8)	2.704(4)
P(1b)–O(21)	1.544(9)	Na(2a)–O(3)	2.871(3)	Na(3b)–O(4)	2.546(3)	⟨Na(5a)–O⟩	2.458
P(1b)–O(21″)	1.595(8)	⟨Na(2a)–O⟩	2.519	Na(3b)–O(7)	2.580(3)		
P(1b)–O(21′)	1.78(3)			Na(3b)–O(20)	2.870(4)	Na(5b)–O(21)	2.261(10)
⟨P(1b)–O⟩	1.514/1.57/1.527[1]	Na(2b)–O(2)	2.245(3)	⟨Na(3b)–O⟩	2.47/2.511[3]	Na(5b)–O(22)	2.276(8)
		Na(2b)–O(15)	2.372(3)			Na(5b)–O(24)	2.299(6)
Na(1a)–O(24)	2.248(5)	Na(2b)–O(17)	2.389(3)	Na(4a)–O(26)	2.122(6)	Na(5b)–O(20)	2.356(5)
Na(1a)–O(3)	2.332(3)	Na(2b)–O(2)	2.389(3)	Na(4a)–O(28)	2.17(5)	Na(5b)–O(21′)	2.38(3)
Na(1a)–O(18)	2.393(3)	Na(2b)–O(15)	2.534(3)	Na(4a)–O(22)	2.302(5)	Na(5b)–O(7)	2.432(5)
Na(1a)–O(5)	2.420(3)	Na(2b)–O(13)	2.837(3)	Na(4a)–O(5)	2.393(4)	Na(5b)–O(21″)	2.516(10)
Na(1a)–O(7)	2.460(3)	⟨Na(2b)–O⟩	2.461	Na(4a)–O(24)	2.560(7)	⟨Na(5b)–O⟩	2.33/2.35/2.38[1]
Na(1a)–O(9)	2.751(3)			Na(4a)–O(25)	2.798(6)		
Na(1a)–O(11)	2.815(3)			Na(4a)–O(24)	2.839(7)	Na(5b′)–O(21)	2.134(12)
⟨Na(1a)–O⟩	2.488			⟨Na(4a)–O⟩	2.502/2.51[4]	Na(5b′)–O(24)	2.215(7)
						Na(5b′)–O(20)	2.329(7)
						Na(5b′)–O(21′)	2.32(3)
						Na(5b′)–O(21″)	2.409(11)
						Na(5b′)–O(7)	2.587(6)
						Na(5b′)–O(22)	2.709(8)
						Na(5b′)–O(11)	2.718(8)
						⟨Na(5b′)–O⟩	2.45/2.48/2.49[1]

Na–O distances are included up to 2.9 Å.
[1] Calculated for polyhedra with bonds M-–O(21)/M–O(21′)/M–O(21″);
[2] Calculated for polyhedra with bonds M–O(23) and M–O(26)/M–O(27) and M–O(28);
[3] Calculated for polyhedra with bonds M–O(21)/M–O(21″);
[4] Calculated for polyhedra with bonds M–O(26)/M–O(28);
[5] Calculated for polyhedra with bonds M–O(23) and M–O(21)/M–O(23) and M–O(21′)/M–O(27) and M–O(21)/M–O(27) and M–O(21′).

Na(5b) and Na(5b′) with the total occupancy much higher than the occupancy of the Na(5a) site (Table 8). The Na (1a)-Na(5b′) and Na(1b)–Na(5a) distances [2.85 and 2.67 Å, respectively] are shorter than the Na(1)–Na(5) distance in lomonosovite (3.16 Å, Cámara *et al.* 2008).

The P(1a) site is split along the *a* axis into two subsites P (1a) and P(1a′) with the occupancies of 87 and 13%, respectively. The respective PO_4 tetrahedra share an edge (*i.e.*, two vertices; Fig. 5b). The P(1b) site is non-split, but the distortion of the P(1b)O_4 tetrahedron is observed with the splitting of the O(21) vertex site into three subsites: O (21), O(21′) and O(21″) with occupancies of 42, 16 and 42%, respectively, and interatomic distances between them ranging from 0.5 to 0.7 Å.

Elongated P–O distances for the O(23), O(27), O(26), O (28), O(21), O(21′) and O(21″) sites and bond-valence calculations indicate that there are several partially protonated anion sites in the structure: two vertices in the P(1)O_4 group [O(23)/O(27) and O(26)/O(28), 1.30/0.08 and 1.45/0.09 vu (valence units)] and one vertex in the P (1b)O_4 group [split O(21) site with in total 1.56 vu] as well as Ti–O–Ti bridging O atoms in the *O* sheet O(17) [1.70 vu] and O(18) [1.79 vu, Tables 4 and 9]. The O(22) [with a P (1b)–O(22) distance of 1.49 Å and a bond valence of 1.80 vu] and O(25) [with P(1b)–O(25) distance of 1.50 Å and 1.78 vu] sites are likely to be O-occupied, possibly with a minor admixture of OH (Tables 4 and 9). Thus the presence of both $PO_2(OH)_2$ and $PO_3(OH)$ groups is most likely in ST4992: the P(1a)$O_2(OH)_2$ [the O(19) and O(24) sites are occupied by O] and P(1b)$O_3(OH)$ groups.

The formula of betalomonosovite for sample ST4992 obtained from the structure refinement is

$$\{Na_{1.71}(Ti_{1.60}Fe^{3+}_{0.40})O_{2.88}(OH)_{1.22}\}\{Na_{1.21}Ca_{0.19}(Ti_{1.88}Mg_{0.08}Nb_{0.04})[Si_2O_7]_2\}\{Na_{3.69}Ca_{0.27}[P_{2.00}O_{6.23}(OH)_{1.77}]\},$$

Table 5. Selected interatomic distances (Å) for betalomonosovite sample Ko0151.

P–O(11)	1.473(5)	Na(2)–O(5)	2.237(5)	Na(3′)–O(13′)	2.10(5)
P–O(10)	1.514(4)	Na(2)–O(1)	2.369(4)	Na(3′)–O(13)	2.155(19)
P–O(12)	1.534(5)	Na(2)–O(5)	2.401(4)	Na(3′)–O(11)	2.303(15)
P–O(13)	1.535(6)	Na(2)–O(2)	2.410(4)	Na(3′)–O(7)	2.473(17)
⟨P–O⟩	1.514	Na(2)–O(1)	2.521(4)	Na(3′)–O(6)	2.54(2)
		Na(2)–O(4)	2.844(4)	Na(3′)–O(10)	2.66(2)
P′–O(12)	1.468(8)	⟨Na(2)–O⟩	2.464	Na(3′)–O(10)	2.73(2)
P′–O(11)	1.469(8)			Na(3′)–O(9)	2.796(13)
P′–O(10)	1.488(11)	Na(3)–O(13′)	2.04(5)	Na(3′)–O(8)	2.879(19)
P′–O(13’)	1.50(5)	Na(3)–O(11)	2.215(15)	⟨Na(3′)–O⟩	2.57/2.56[1]
⟨P′–O⟩	1.48	Na(3)–O(13)	2.315(19)		
		Na(3)–O(6)	2.375(16)	Na(4)–O(13)	2.168(9)
Na(1)–O(12)	2.249(6)	Na(3)–O(10)	2.46(2)	Na(4)–O(11)	2.198(7)
Na(1)–O(2)	2.471(5)	Na(3)–O(7)	2.615(16)	Na(4)–O(3)	2.365(6)
Na(1)–O(9)	2.565(7)	Na(3)–O(8)	2.830(11)	Na(4)–O(12)	2.407(9)
Na(1)–O(6)	2.603(5)	⟨Na(3)–O⟩	2.47/2.42[1]	*Na(4)–O(12)*	*2.912(7)*
Na(1)–O(8)	2.614(7)			⟨Na(4)–O⟩	2.410
Na(1)–O(7)	2.620(5)				
Na(1)–O(3)	2.643(5)			Na(5)–O(13)	2.189(8)
Na(1)–O(3)	2.705(5)			Na(5)–O(12)	2.242(5)
<Na(1)–O>	2.559			Na(5)–O(13′)	2.26(5)
				Na(5)–O(10)	2.406(5)
				Na(5)–O(6)	2.498(5)
				Na(5)–O(11)	2.631(9)
				Na(5)–O(7)	2.791(5)
				⟨Na(5)–O⟩	2.460/2.47[1]

Na–O distances are included up to 2.9 A except special cases.
[1] Calculated for polyhedra with bonds M–O(13)/M–O(13′).

Table 6. Selected interatomic distances (Å) for betalomonosovite sample GIM6019.

P(1a)–O(24)	1.493(9)	Na(1b)–O(25)	2.271(11)		Na(3a)–O(28)	2.18(4)	Na(4b)–O(23)	2.22(2)
P(1a)–O(19)	1.519(7)	Na(1b)–O(12)	2.404(7)		Na(3a)–O(26)	2.197(12)	Na(4b)–O(27)	2.22(5)
P(1a)–O(23)	1.529(9)	Na(1b)–O(10)	2.405(7)		Na(3a)–O(23)	2.396(12)	Na(4b)–O(6)	2.303(17)
P(1a)–O(26)	1.538(10)	Na(1b)–O(6)	2.459(7)		Na(3a)–O(27)	2.41(5)	Na(4b)–O(21)	2.31(3)
⟨P(1a)–O⟩	1.520	Na(1b)–O(17)	2.649(7)		Na(3a)–O(8)	2.418(6)	Na(4b)–O(25)	2.60(2)
		Na(1b)–O(8)	2.703(7)		Na(3a)–O(19)	2.468(7)	Na(4b)–O(25)	2.77(2)
P(1a′)–O(27)	1.49(2)	⟨Na(1b)–O⟩	2.48		Na(3a)–O(12)	2.558(7)	⟨Na(4b)–O⟩	2.44/2.44[4]
P(1a′)–O(28)	1.498(19)				Na(3a)–O(9)	2.689(7)		
P(1a′)–O(24)	1.510(18)	Na(2a)–O(1)	2.231(7)		⟨Na(3a)–O⟩	2.45/2.45[2]	Na(5a)–O(28)	2.17(4)
P(1a′)–O(19)	1.510(17)	Na(2a)–O(16)	2.378(7)				Na(5a)–O(25)	2.187(11)
⟨P(1a′)–O⟩	1.50	Na(2a)–O(1)	2.410(7)		Na(3b)–O(21)	2.12(4)	Na(5a)–O(26)	2.310(12)
		Na(2a)–O(18)	2.412(7)		Na(3b)–O(22)	2.283(12)	Na(5a)–O(23)	2.410(12)
P(1b)–O(22)	1.491(9)	Na(2a)–O(16)	2.539(7)		Na(3b)–O(21′)	2.331(19)	Na(5a)–O(19)	2.480(9)
P(1b)–O(25)	1.500(9)	Na(2a)–O(14)	2.796(7)		Na(3b)–O(11)	2.431(6)	Na(5a)–O(12)	2.495(8)
P(1b)–O(20)	1.513(6)	Na(2a)–O(3)	2.880(7)		Na(3b)–O(20)	2.469(8)	Na(5a)–O(27)	2.50(4)
P(1b)–O(21′)	1.54(2)	⟨Na(2a)–O⟩	2.521		Na(3b)–O(7)	2.548(6)	Na(5a)–O(8)	2.601(8)
P(1b)–O(21)	1.60(2)				Na(3b)–O(4)	2.600(7)	⟨Na(5a)–O⟩	2.41/2.41[2]
⟨P(1b)–O⟩	1.53/1.51[1]	Na(2b)–O(2)	2.249(7)		⟨Na(3b)–O⟩	2.41/2.44[1]		
		Na(2b)–O(15)	2.363(6)				Na(5b)–O(21)	2.09(3)
Na(1a)–O(24)	2.252(11)	Na(2b)–O(17)	2.382(6)		Na(4a)–O(22)	2.181(16)	Na(5b)–O(24)	2.164(10)
Na(1a)–O(5)	2.387(7)	Na(2b)–O(2)	2.397(7)		Na(4a)–O(26)	2.187(17)	Na(5b)–O(21′)	2.39(3)
Na(1a)–O(3)	2.389(8)	Na(2b)–O(15)	2.496(7)		Na(4a)–O(28)	2.24(5)	Na(5b)–O(20)	2.403(8)
Na(1a)–O(7)	2.416(7)	Na(2b)–O(13)	2.872(7)		Na(4a)–O(5)	2.380(13)	Na(5b)–O(7)	2.406(8)
Na(1a)–O(18)	2.504(7)	⟨Na(2b)–O⟩	2.460		Na(4a)–O(24)	2.621(18)	Na(5b)–O(22)	2.529(17)
Na(1a)–O(11)	2.771(7)				Na(4a)–O(25)	2.693(16)	Na(5b)–O(11)	2.841(10)
Na(1a)–O(9)	2.798(8)				Na(4a)–O(24)	2.746(18)	⟨Na(5b)–O⟩	2.41/2.46[1]
⟨Na(1a)–O⟩	2.502				⟨Na(4a)–O⟩	2.47/2.48[3]		

Na–O distances are included up to 2.9 A.
[1] Calculated for polyhedra with bonds M–O(21)/M–O(21′);
[2] Calculated for polyhedra with bonds M–O(23) and M–O(26)/M–O(27) and M–O(28);
[3] Calculated for polyhedra with bonds M–O(26)/M–O(28);
[4] Calculated for polyhedra with bonds M–O(23)/M–O(27).

Table 7. Selected interatomic distances (Å) for betalomonosovite sample OlR019.

P(1a)–O(19)	1.501(6)	Na(1b)–O(25)	2.248(12)	Na(2b)–O(2)	2.280(9)	Na(3b)–O(21)	2.231(10)
P(1a)–O(24)	1.511(9)	Na(1b)–O(10)	2.458(11)	Na(2b)–O(15)	2.364(8)	Na(3b)–O(22)	2.393(11)
P(1a)–O(23)	1.542(8)	Na(1b)–O(12)	2.481(9)	Na(2b)–O(17)	2.382(9)	Na(3b)–O(7)	2.439(8)
P(1a)–O(26)	1.546(9)	Na(1b)–O(6)	2.578(9)	Na(2b)–O(15)	2.420(9)	Na(3b)–O(20)	2.482(8)
⟨P(1a)–O⟩	1.525	Na(1b)–O(8)	2.634(10)	Na(2b)–O(2)	2.424(9)	Na(3b)–O(11)	2.499(9)
		Na(1b)–O(17)	2.717(8)	*Na(2b)–O(4)*	*2.989(11)*	Na(3b)–O(4)	2.813(10)
P(1b)–O(25)	1.491(10)	Na(1b)–O(6)	2.790(9)	*Na(2b)–O(13)*	*2.992(9)*	⟨Na(3b)–O⟩	2.48
P(1b)–O(20)	1.506(7)	Na(1b)–O(4)	2.868(12)	⟨Na(2b)–O⟩	2.55		
P(1b)–O(22)	1.519(8)	⟨Na(1b)–O⟩	2.60			Na(5a)–O(25)	2.061(12)
P(1b)–O(21)	1.557(8)			Na(3a)–O(26)	2.259(10)	Na(5a)–O(23)	2.309(11)
⟨P(1b)–O⟩	1.52	Na(2a)–O(1)	2.266(10)	Na(3a)–O(23)	2.380(11)	Na(5a)–O(26)	2.334(12)
		Na(2a)–O(16)	2.378(9)	Na(3a)–O(19)	2.439(8)	Na(5a)–O(12)	2.371(10)
Na(1a)–O(24)	2.252(12)	Na(2a)–O(18)	2.408(9)	Na(3a)–O(8)	2.465(9)	Na(5a)–O(8)	2.555(11)
Na(1a)–O(7)	2.443(8)	Na(2a)–O(16)	2.425(9)	Na(3a)–O(12)	2.477(8)	Na(5a)–O(19)	2.589(10)
Na(1a)–O(5)	2.504(9)	Na(2a)–O(1)	2.430(9)	Na(3a)–O(9)	2.836(10)	⟨Na(5a)–O⟩	2.37
Na(1a)–O(3)	2.527(13)	*Na(2a)–O(3)*	*2.928(11)*	⟨Na(3a)–O⟩	2.48		
Na(1a)–O(18)	2.695(8)	*Na(2a)–O(14)*	*2.952(9)*			Na(5b)–O(24)	2.054(12)
Na(1a)–O(11)	2.718(10)	⟨Na(2a)–O⟩	2.54			Na(5b)–O(21)	2.288(12)
Na(1a)–O(9)	2.787(12)					Na(5b)–O(7)	2.308(10)
Na(1a)–O(5)	2.862(9)					Na(5b)–O(22)	2.407(12)
⟨Na(1a)–O⟩	2.60					Na(5b)–O(20)	2.564(10)
						Na(5b)–O(11)	2.634(11)
						⟨Na(5b)–O⟩	2.38

Na–O distances are included up to 2.9 A except special cases.

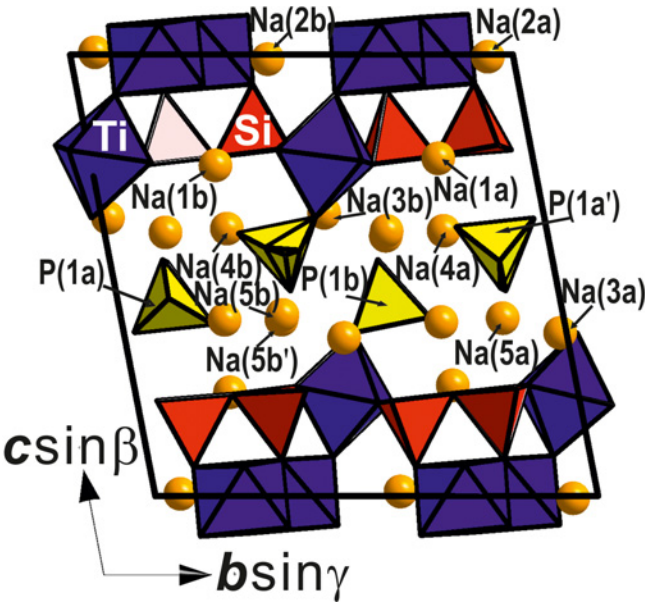

Fig. 4. General view of the crystal structure of betalomonosovite: sample ST4992. The unit cell is outlined.

where the contents of the *O* and *H* sheets and the interlayer space are given in braces. The simplified formula can be written as $Na_7Ti_4[Si_2O_7]_2[PO_3(OH)]_2O_3(OH)$. Here the $[PO_3(OH)]_2$ part reflects the degree of protonation only, not the type of H-bearing groups. The actually observed situation corresponds to the formula $\{PO_2[O_{x}(OH)_{2-x}]/PO_2[O_{2-x}(OH)_x]\}\{PO_3[O_x(OH)_{1-x}]/PO_3[O_{1-x}(OH)_x]\}$ where OH groups statistically replace O in one or two anion sites (Table 10).

5.3.2. Sample Ko0151

Five cation sites in the crystal structure of Ko0151 have the same or slightly lower occupancies than their topological analogues in the structure of ST4992 (Fig. S1). Again, the Na(3) site shows the highest total occupancy, though it is split into Na(3) and Na(3′) subsites with occupancies of 61 and 38%, respectively (Table 8). An admixture of Mn (0.1 atom *pfu*) was introduced into several large-cation sites in order to correlate structural data with the observed chemical composition. The Na(1)–Na(5) distance is 2.71 Å. The P site is also split into two subsites, P and P′, with occupancies of 89 and 11%, respectively. The respective PO_4 and $P'O_4$ tetrahedra share three vertices, *i.e.* a face (Fig. 5c).

According to the bond-valence sums, several anionic sites show partial substitution of O^{2-} by OH^-. These are the O(12) [1.72 vu] and O(13)/O(13′) [1.59/0.07 vu] sites of the phosphate tetrahedra and Ti–O–Ti bridging O(2) atom in the *O* sheet [1.66 vu, Table 9].

The formula of betalomonosovite for sample Ko0151 obtained from the structure refinement is

$$\{Na_{1.46}(Ti_{1.48}Fe^{3+}_{0.30}Nb_{0.14}Mn_{0.08})O_{2.74}(OH)_{0.99}F_{0.27}\}$$
$$\{Na_{0.74}Ca_{0.22}Mn_{0.10}(Ti_{1.64}Nb_{0.18}Mg_{0.18})[Si_2O_7]_2\}$$
$$\{Na_{3.64}Ca_{0.22}Mn_{0.10}[P_{2.00}O_{5.88}(OH)_{2.12}]\},$$

where the contents of the *O* and *H* sheets and the interlayer space are given in braces. The fluorine content is given according to the electron microprobe data. The simplified

Table 8. Site occupancies for Na and P sites in the structures of betalomonosovite samples ST4992, Ko0151, GIM6019 and OIR0194, as compared to lomonosovite.

Lomonosovite[1]		Betalomonosovite							
		ST4992		Ko0151		GIM6019		OIR0194	
Site	site occupancy	site	site occupancy[2]	site	site occupancy[2]	site	site occupancy[2]	site	site occupancy[2]
P	1	P(1a)	[13.0] $P_{0.868(8)}$	P	[13.4] $P_{0.894(7)}$	P(1a)	[12.1] $P_{0.809(13)}$	P(1a)	1
		P(1a′)	[2.0] $P_{0.132(8)}$	P′	[1.6] $P_{0.106(7)}$	P(1a′)	[2.9] $P_{0.191(13)}$		
		P(1b)	1			P(1b)	1	P(1b)	1
Na(1)	$Na_{0.975}$	Na(1a)	[8.5] $Na_{0.60}Ca_{0.09}$	Na(1)	[7.5] $Na_{0.37}Ca_{0.11}Mn_{0.05}$	Na(1a)	[7.9] $Na_{0.43}Ca_{0.16}$	Na(1a)	[7.8] $Na_{0.51}Ca_{0.11}$
		Na(1b)	[8.7] $Na_{0.61}Ca_{0.10}$			Na(1b)	[7.9] $Na_{0.38}Ca_{0.11}Mn_{0.06}$	Na(1b)	[7.9] $Na_{0.52}Ca_{0.11}$
Na(2)	$Na_{0.975}$	Na(2a)	[9.4] $Na_{0.856(8)}$	Na(2)	[8.0] $Na_{0.733(9)}$	Na(2a)	[8.0] $Na_{0.730(16)}$	Na(2a)	[5.9] $Na_{0.537(17)}$
		Na(2b)	[9.5] $Na_{0.860(8)}$			Na(2b)	[8.3] $Na_{0.760(16)}$	Na(2b)	[5.6] $Na_{0.507(16)}$
Na(3)	$Na_{0.945}Ca_{0.55}$	Na(3a)	[10.8] $Na_{0.985(9)}$	Na(3)	[6.7] $Na_{0.61(6)}$	Na(3a)	[10.9] $Na_{0.993(18)}$	Na(3a)	[10.5] $Na_{0.962(18)}$
				Na(3′)	[4.2] $Na_{0.38(6)}$				
		Na(3b)	[9.2] $Na_{0.836(8)}$			Na(3b)	[10.5] $Na_{0.960(17)}$	Na(3b)	[10.4] $Na_{0.952(19)}$
Na(4)	$Na_{0.855}Mn_{0.08}$	Na(4a)	[4.8] $Na_{0.438(8)}$	Na(4)	[4.8] $Na_{0.438(10)}$	Na(4a)	[2.9] $Na_{0.261(15)}$		
		Na(4b)	[4.4] $Na_{0.403(8)}$			Na(4b)	[2.3] $Na_{0.213(16)}$		
Na(5)	1	Na(5a)	[6.6] $Na_{0.44}Ca_{0.09}$	Na(5)	[7.7] $Na_{0.39}Ca_{0.11}Mn_{0.05}$	Na(5a)	[6.0] $Na_{0.31}Ca_{0.09}Mn_{0.03}$	Na(5a)	[4.6] $Na_{0.20}Ca_{0.12}$
		Na(5b)	[5.8] $Na_{0.36}Ca_{0.09}$						
		Na(5b′)	[4.3] $Na_{0.23}Ca_{0.09}$			Na(5b)	[8.0] $Na_{0.49}Ca_{0.13}$	Na(5b)	[4.8] $Na_{0.22}Ca_{0.12}$

[1] After Cámara *et al.*, 2008
[2] Based on the e_{ref} values (given in square brackets) and electron microprobe data

formula is $Na_6Ti_4[Si_2O_7]_2[PO_3(OH)]_2O_2(OH,F)_2$. The structural data give approximately 6.5 large cations *pfu*, rounded down to 6 for the better agreement with the chemical data. As in the previous case, the formally written $[PO_3(OH)]_2$ part can be specified as $\{PO_2[O_x(OH)_{2-x}]/PO_2[O_{2-x}(OH)_x\}_2$, where OH groups statistically replace O^{2-} in one or two anion sites (Table 10).

5.3.3. Sample GIM6019

There are ten large-cation sites in the structure of GIM6019 with Na(3a) and Na(3b) being almost fully occupied, whereas eight other sites show significant deficiency compared to sample ST4992 with the Na(4a) and Na(4b) sites being mostly vacant (occupancies of 26 and 21%, respectively; Table 8, Fig. S2). The P(1a) site is split into two subsites, P(1a) and P(1a′), with occupancies of 81 and 19%, respectively, and the P(1a)O_4 and P(1a')O_4 tetrahedra sharing a common edge. The P(1b)O_4 tetrahedron is distorted: the O(21) site is split into two subsites, O(21) and O(21′) (with occupancies of 51 and 49%, respectively, Fig. 5d). As in the ST4992 sample, "paired" sites generally have roughly similar occupancies with the exception of the Na (5a) and Na(5b) pair, where the Na(5b) site has a higher occupancy (Table 8). The Na(1a)–Na(5b) and Na(1b)–Na (5a) distances are shortened (2.61 and 2.34 Å, respectively), which means that the Na(1b) and Na(5a) sites are statistically occupied. The structural data obtained allowed us to confirm such an arrangement by making those sites partially occupied by Ca and Mn. A similar substitution was introduced for all obtained models.

The composition of the anion in the structures of GIM6019 and ST4992 are similar, though the GIM6019 sample shows a higher degree of protonation of the O sites. Two anion sites in the P(1)O_4 group are likely to be OH-dominant [O(23)/O(27) and O(26)/O(28), 1.11/0.13 and 1.23/0.19 vu], while, in the P(1b)O_4 group, one anion site has mixed O/OH occupancy [split O(21) site with a total 1.69 vu]. The O(17) and O(18) sites at the Ti–O–Ti bridges also show lower bond-valence sums: 1.60 and 1.65, respectively (Table 9). The O(22) [with P(1b)–O (22) distance of 1.49 Å and 1.72 vu] and O(25) [with P (1b)–O(25) distance of 1.50 Å and 1.77 vu] sites are likely to be O-occupied or with a small admixture of OH^- (Tables 6 and 9). Thus both $PO_2(OH)_2$ and $PO_3(OH)$ groups are likely to be present in the structure of GIM6019.

The formula obtained from the structure refinement of sample GIM6019 is

$$\{Na_{1.49}(Ti_{1.45}Fe^{3+}_{0.55})O_{2.37}(OH)_{1.63}\}$$
$$\{Na_{0.81}Ca_{0.27}Mn_{0.06}(Ti_{1.84}Mg_{0.10}Nb_{0.06})[Si_2O_7]_2\}$$
$$\{Na_{3.22}Ca_{0.22}Mn_{0.03}[P_{2.00}O_{5.62}(OH)_{2.38}]\},$$

where the contents of the *O* and *H* sheets and the interlayer space are given in braces. The simplified formula is $Na_6Ti_4[Si_2O_7]_2[PO_3]_2O_2(OH)_2$. As in the ST4992 sample, the $[PO_3(OH)]_2$ part can be written as $\{PO_2[O_x(OH)_{2-x}]/$

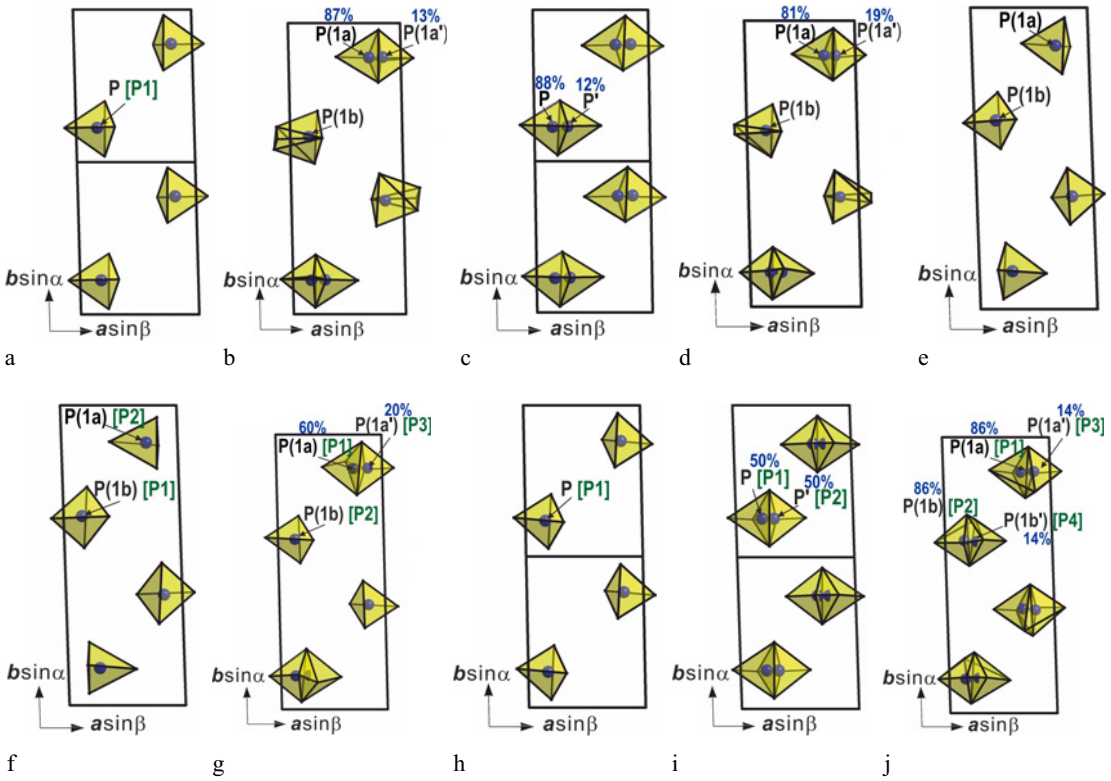

Fig. 5. Phosphate groups in the structures of lomonosovite (a), after Cámara *et al.*, 2008, and betalomonosovite samples ST4992 (b), GIM6019 (c), OlR0194 (d) and Ko0151 (e) as compared to data reported by Rastsvetaeva *et al.*, 1975 (f), Rastsvetaeva, 1986 (g), Khalilov, 1990 (h), Yakubovich *et al.*, 2014 (i) and Sokolova *et al.*, 2015a (j). All projections are along *c*. Unit cells are outlined. Numbers show site occupancies; in square brackets the original site labels are given.

$PO_2[O_{2-x}(OH)_x]\}\{PO_3[O_x(OH)_{1-x}]/PO_3[O_{1-x}(OH)_x]\}$, where OH groups statistically replace O^{2-} in one or two anion sites (Table 10).

5.3.4. Sample OlR0194

There are only eight large-cation sites in the crystal structure of OlR0194 with the Na(4a) and Na(4b) sites being vacant (Fig. S3). The Na(3a) and Na(3b) sites are almost fully occupied, while the occupancies of the Na (2a), Na(2b), Na(5a) and Na(5b) sites are noticeably lower than in all structures considered above. This results in only *ca.* five large cations *pfu* (Table 8). The structure is characterized by shortened Na(1a)–Na(5b) [2.07 Å] and Na(1b)–Na(5a) [2.03 Å] interatomic distances, *i.e.* the respective sites are statistically occupied.

In this model, none of the P sites is split (Fig. 5e), but there are several residual electron-density peaks in the final difference map located around P(1b) [1.83 e/Å^3] and P(1a) [1.13 e/Å^3]. Therefore, both sites can be considered as split into two sites each, but the model cannot be refined due to unstability. One of the PO_4 tetrahedra is reversed compared to lomonosovite (Fig. 5a (Cámara *et al.* 2008)) resulting in the doubling of the unit cell.

There are two anion sites with mixed OH/O occupancy [O(23) and O(26) with 1.49 vu and 1.55 vu, respectively] and one fully O-occupied site [O(19), 1.95 vu] in the P(1a) O_4 group. The fourth anion site O(24) with 1.71 vu and the P–O distance of 1.51 Å is likely to have a small admixture of OH^-. In the P(1b)O_4 group, two anion sites have mixed O/OH occupancy with the bond-valence sums of 1.53 vu [O(22), P–O distance is 1.52 Å] and 1.43 vu [O(21), P–O distance is 1.56 Å], and two other sites O-occupied [O(20) and O(25), Tables 7, 9]. Bond-valence sums for the O(17) and O(18) anions at the Ti–O–Ti bridges are 1.46 and 1.45 vu, respectively, which shows the highest degree of protonation among all studied samples (Table 9).

The formula obtained from the structure refinement of sample OlR0194 is

$$\begin{array}{l}\{Na_{1.04}(Ti_{1.42}Fe^{3+}_{0.46}Mn_{0.12})O_{1.60}(OH)_{2.40}\}\\ \{Na_{1.03}Ca_{0.22}(Ti_{1.74}Mg_{0.16}Nb_{0.10})[Si_2O_7]_2\}\\ \{Na_{2.33}Ca_{0.24}[P_{2.00}O_{4.80}(OH)_{3.20}]\},\end{array}$$

where the contents of the *O* and *H* sheets and the interlayer space are given in braces. The simplified formula is $Na_5Ti_4[Si_2O_7]_2[PO_{22}][PO_3(OH)]O_2(OH)_2$. The formally written $[PO_2(OH)_2][PO_3(OH)]$ part can be specified as $\{PO_2[O_x(OH)_{2-x}]/PO_2[O_{2-x}(OH)_x]\}\{PO_2[O_x(OH)_{2-x}]/PO_2[O_{2-x}(OH)_x]\}$ where OH groups statistically replace O^{2-} in one or two anion sites (Table 10).

Table 9. Bond-valence sums (BVS) for the anions in the phosphate groups and in the Ti–O–Ti bridges in the structure of betalomonosovite samples ST4992, GIM6019, OlR0194 and Ko0151.

	ST4992		GIM6019		OlR0194			Ko0151	
	site	BVS	site	BVS	site	BVS		site	BVS
P(1a)	O(23)/O(27)	1.30/0.08	O(23)/O(27)	1.11/0.13	O(23)	1.49	P	O(10)	1.99
	O(26)/O(28)	1.45/0.09	O(26)/O(28)	1.23/0.19	O(26)	1.55			
	O(19)	1.93	O(19)	1.90	O(19)	1.95		O(11)	1.94
	O(24)	1.86	O(24)	1.87	O(24)	1.71			
P(1b)	O(20)	2.01	O(20)	1.97	O(20)	1.91		O(12)	1.72
	O(22)	1.80	O(22)	1.72	O(22)	1.53			
	O(25)	1.78	O(25)	1.77	O(25)	1.78		O(13)/O(13′)	1.59/0.07
	O(21)/O(21′)/O(21″)	0.85/0.15/0.56	O(21)/O(21′)	0.93/0.76	O(21)	1.43			
Ti–O–Ti	O(17)	1.70	O(17)	1.60	O(17)	1.46	Ti–O–Ti	O(2)	1.66
Ti–O–Ti	O(18)	1.79	O(18)	1.65	O(18)	1.45			

6. Discussion

6.1. Crystal chemistry and formation mechanism of betalomonosovite

The obtained data show significant chemical and structural variations of betalomonosovite. In the ST4992–[Ko0151–GIM6019]–OlR0194 series, the amount of large cations (with major, species-defining Na) *decreases*, whereas the degree of substitution of O^{2-} by OH^{-} in P-centered tetrahedra and at Ti–O–Ti bridges in the *O* sheet *increases*. Some structural features are the same in all structures, namely:

– occupancies of the almost fully occupied Na(3) sites remain unchanged in all models;
– the Na(4) sites have the lowest occupancies, down to zero in OlR0194, and occupancies of the Na(5) sites are also decreasing consistently;
– the Na(1)–Na(5) interatomic distances are shortened down to 2.0–2.1 Å in OlR0194 (*i.e.*, Na-centered polyhedra are shifting adjusting to the changes in the interlayer space), which makes them statistically occupied;
– in the structures with the doubled *b* parameter, "paired" sites have roughly similar occupancies with the exception of the Na(5a) and Na(5b) pair, where the Na(5b) site has a higher occupancy in ST4992 and GIM6019 (Table 8);
– one anion site in each PO_4 group [*i.e.* the O(19) and O(20) sites belonging to coordination polyhedra of the Ti(1) sites in the *H* sheet] remains occupied solely by O^{2-}.

On the other hand, some crystal-chemical features show considerable variability such as splitting of P, O and large-cation sites and protonation of oxygen atoms.

The occurrence of the partial pseudomorphs of betalomonosovite after lomonosovite was confirmed by (a) IR spectroscopy, which showed the formation of acid phosphate groups in the newly formed phase and (b) megascopic and microscopic observations, which showed a lower content of sodium but almost unchanged content of phosphorus in the replacing phase. These data provide a direct proof of the secondary nature of betalomonosovite and allow considering it as a "transformation mineral species" (Khomyakov, 1995), *i.e.* a mineral that does not crystallize directly from a melt or a solution but forms exclusively by replacing a protomineral with preservation of its stable structure motifs (*HOH* blocks in our case). We believe that betalomonosovite in all cases is a product of alteration (partial Na leaching with protonation of some O anions) of primary lomonosovite; no convincing evidence of the hypothesis that betalomonosovite can crystallize directly from a fluid has been reported in literature or found by us.

Betalomonosovite seems to be a mineral "flexible" in both chemical and structural aspects: in each case we register a phase slightly different in terms of degree and character of the original lomonosovite alteration. We consider all above-discussed samples as different varieties of the same mineral species betalomonosovite.

The ST4992 and GIM6019 samples are definitely the products of different stages of lomonosovite alteration formed by similar mechanisms. Both demonstrate the *b*-doubled unit cell and in both cases the P(1a) site is split into two subsites with similar occupancies, while the P(1b) O_4 groups are distorted with the O(21) vertices split into subsites. The content of large cations and the degree of protonation of oxygen atoms are consistently different for these samples: ST4992 is a product of a less advanced stage of alteration of lomonosovite alteration compared to GIM6019. The sample studied by Rastsvetaeva (1986) is most likely a product of the same scheme of betalomonosovite formation (Fig. 5g).

The Ko0151 sample is characterized by a roughly similar degree of protonation and Na leaching as GIM6019, but its formation mechanism seems to be different, resulting in the symmetrical splitting of both P sites and the leaching of Na [hence the introduction of the small, lomonosovite-type unit cell]. Similar site splitting was reported by Yakubovich *et al.* (2014), but in the latter case: (a) both P subsites are half-occupied and (b) statistically occupied PO_4 tetrahedra are "inserted" into each other sharing an edge (as in the structures of ST4992 and GIM6019), while in the structure of Ko0151 they share three oxygen vertices, *i.e.* a face (Fig. 5c, i).

Table 10. Simplified and detailed structural formulae of betalomonosovite samples ST4992, Ko0151, GIM6019 and OlR0194

Sample	Simplified formula	Phosphate groups composition*	*HOH* block	Interlayer space
ST4992	$Na_7Ti_4[Si_2O_7]_2[PO_3(OH)]_2O_3(OH)$.	$\{PO_2[O_x(OH)_{2-x}]/PO_2[O_{2-x}(OH)_x]\}$ $\{PO_3[O_x(OH)_{1-x}]/PO_3[O_{1-x}(OH)_x]\}$	$Na_{2.92}Ca_{0.19}(Ti_{3.48}Fe^{3+}_{0.40}Nb_{0.08}Mg_{0.04})$ $[Si_2O_7]_2O_{2.88}(OH)_{1.22}$	$Na_{3.69}Ca_{0.27}[P_{2.00}O_{6.23}(OH)_{1.77}]$
Ko0151	$Na_6Ti_4[Si_2O_7]_2[PO_3(OH)]_2O_2(OH)_2$	$\{PO_2[O_x(OH)_{2-x}]/PO_2[O_{2-x}(OH)_x]_2$	$Na_{2.20}Ca_{0.22}Mn_{0.10}(Ti_{3.12}Nb_{0.32}Fe^{3+}_{0.30}Mn_{0.08}Mg_{0.18})$ $[Si_2O_7]_2O_{2.74}(OH)_{0.99}F_{0.27}$	$Na_{3.64}Ca_{0.22}Mn_{0.10}[P_{2.00}O_{5.88}(OH)_{2.12}]$
GIM6019	$Na_6Ti_4[Si_2O_7]_2[PO_3(OH)]_2O_2(OH)_2$	$\{PO_2[O_x(OH)_{2-x}]/PO_2[O_{2-x}(OH)_x]\}$ $\{PO_3[O_x(OH)_{1-x}]/PO_3[O_{1-x}(OH)_x]\}$	$Na_{2.30}Ca_{0.27}Mn_{0.06}(Ti_{3.29}Fe^{3+}_{0.55}Mg_{0.1}Nb_{0.06})$ $[Si_2O_7]_2O_{2.47}(OH)_{1.63}$	$Na_{3.22}Ca_{0.22}Mn_{0.03}[P_{2.00}O_{5.62}(OH)_{2.38}]$
OlR0194	$Na_5Ti_4[Si_2O_7]_2[PO_2(OH)_2][PO_3(OH)]O_2(OH)_2$	$\{PO_2[O_x(OH)_{2-x}]/PO_2[O_{2-x}(OH)_x]\}$ $\{PO_2[O_x(OH)_{2-x}]/PO_2[O_{2-x}(OH)_x]\}$	$Na_{2.07}Ca_{0.22}(Ti_{3.16}Fe^{3+}_{0.46}Mg_{0.16}Mn_{0.12}Nb_{0.10})$ $[Si_2O_7]_2\}O_{1.60}(OH)_{2.40}$	$Na_{2.33}Ca_{0.24}[P_{2.00}O_{4.80}(OH)_{3.20}]$

* Formulae represent possible composition of phosphate groups with OH-groups statistically replacing O in one or two anion sites.

Similar transformations were observed by us in ion-exchange experiments with lomonosovite at 150 °C, when its Ag- and Cu-exchanged forms were obtained (Lykova *et al.* 2015): splitting of the P sites to form statistically occupied PO_4 tetrahedra sharing three vertices was observed in both structures. However, only one of the two P sites is split in the Ag-exchanged form of lomonosovite (hence the choice a unit cell doubled along the *b* axis), while in the Cu-exchanged form both P sites are split, therefore the unit cell is preserved as a lomonosovite-type one. The protonation / deprotonation of oxygen atoms at the Ti–O–Ti bridges also proved to be an important and sensitive charge-balancing mechanism in cation-exchanged forms of lomonosovite.

The sample OlR0194 should be considered as a product of the deep alteration of lomonosovite: it shows the highest degree of protonation of O atoms and the lowest Na content. It also has the *b*-doubled unit cell due to the reversed position of one of the PO_4 tetrahedra compared to lomonosovite. The models obtained by Rastsvetaeva *et al.* (1975) and Sokolova *et al.* (2015a) are very similar to that refined for the OlR0194 sample. The studied phases are likely to be the products of a similar mechanism of lomonosovite alteration (Fig. 5d, f, j).

In accordance with the sequence discussed above, the crystal structure of the sample with the least degree of protonation (ST4992) was refined to an *R* value of 4.32%, while the structure of the sample with the highest degree of protonation (OlR0194) was refined to the relatively high *R* value of 9.55%. This observation reflects the increase of the degree of heterogeneity as the transformation progresses.

In the crystal structure discussed by Khalilov (1990) the arrangement of PO_4 tetrahedra is close to that observed in lomonosovite (Fig. 5h). However, the resultant simplified formula of betalomonosovite in the cited work has an excess charge of +2 (see below), undermining the reliability of the structural data. Thus, we should not consider this model as a product of a different scheme of betalomonosovite formation until more reliable data are obtained.

According to the IR spectroscopic data (Fig. 3), there is a small amount of H_2O molecules in the ST4992, Ko0151 and OlR0194 samples. The protonation of O atoms and the leaching of Na are probably accompanied by hydration with the formation of murmanite, $Na_4Ti_4(Si_2O_7)_2O_4 \cdot 4H_2O$, a PO_4-free heterophyllosilicate with H_2O in the interlayer. The possibility of such a transformation was discussed by Lykova *et al.* (2016).

The presence of the IR bands in the range 2420–2440 cm^{-1} for all four studied samples indicates the presence of P-O-H groups. Similar bands are present in the IR spectra of all acid phosphates and are especially strong in the IR spectra of hydrous acid phosphates. Usually bands in the range 2200–2600 cm^{-1} correspond to the strong hydrogen bonds between P–O–H groups and H_2O molecules (Chukanov & Chervonnyi, 2016).

According to the empirical correlation between O-H stretching frequencies in IR spectra of minerals and O···O distances (from structural data) proposed by Libowitzky (1999, ν (cm^{-1}) = 3592–304 · 10^9 · exp[–*d*(O···O)/

0.1321]), the wavenumbers 2420–2440 cm^{-1} correspond to an O···O distance of about 2.56 Å. However, such short distances are absent in betalomonosovite. It should be noted that the correlation works satisfactorily only in the medium range of wavenumbers (from 2900 to 3550 cm^{-1}). In particular, it predicts that the maximum possible value of the O–H stretching frequencies for minerals is 3592 cm^{-1}. However, *e.g.* for magnesium serpentines, brucite and kaolinite, observed frequencies are close to 3700 cm^{-1}. In the low-frequency region, a strong scatter of experimental data is observed, and relatively small changes of the O···O distances (below 0.1 Å) can result in band shifts of several hundreds cm^{-1} (Chukanov & Chervonnyi, 2016).

6.2. The simplified and the idealized formulae of betalomonosovite

The literature data and our results show significant chemical and structural variations for betalomonosovite, which resemble those observed in zeolites and zeolite-like minerals. By analogy with these materials, betalomonosovite cannot be described with an "end-member" formula. Besides, no data showing the existence of a continuous solid-solution series between lomonosovite and betalomonosovite were reported: lomonosovite is always H-free or almost H-free (only very minor bands corresponding to H-bearing groups were observed in its IR spectra). We conclude that the transformation from lomonosovite to betalomonosovite has a discrete character and results in the formation of the mineral with a minimum of 2H *apfu* in the interlayer (*i.e.*, protonating phosphate groups), without intermediate phases [which could be formally defined as H-bearing varieties of lomonosovite]. This has some bearing on the definition of betalomonosovite as a mineral species. Here the "classical" definition of betalomonosovite given by Sokolova *et al.* (1971) should be recalled, pointing out its *crucial, "fingerprint" features*: the presence of *H* in the form of the acid phosphate anion(s) $[PO_2(OH)_2] \pm [PO_3(OH)]$, with the same content of phosphorous, 2P *apfu*, as in lomonosovite, $Na_{10}Ti_4(Si_2O_7)_2(PO_4)_2O_4$, in contrast to murmanite, $Na_4Ti_4(Si_2O_7)_2O_4{\cdot}4H_2O$, a P-free product of lomonosovite alteration (Borneman-Starynkevich, 1946). Then, summarizing all the above, we can try to define the *scope of variability* corresponding to this mineral.

Two coupled processes determine the formation of betalomonosovite in Nature: leaching of large cations (species-defining Na with admixed K and Ca) and protonation of oxygen atoms. In the *HOH* block the process is limited to the protonation of the Ti–O–Ti bridging oxygen atoms in the *O* sheet. All other O atoms are either connected to Si or saturated predominantly by Ti^{4+} [O(13) and O(14) in the *b*-doubled unit cell and O(4) in the small cell]. Thus the extreme simplified composition of the *HOH* block of betalomonosovite can be written as $Na_2Ti_4[Si_2O_7]_2O_2(OH)_2$ with all Na sites being half-occupied. In the interlayer space, the alteration is limited to the formation of $[PO_2(OH)_2]$ groups with no further protonation possible, for chemical and bond-valence reasons. Thus the composition of the interlayer space can be written as $Na_2[PO_2(OH)_2]_2$ with the Na(3) sites occupied and the Na(4) and Na(5) sites vacant. The OlR0194 sample shows a composition close to the extreme in both aspects. Thus *the idealized formula of the most H-rich betalomonosovite* can be written as $Na_4Ti_4[Si_2O_7]_2[PO_2(OH_2)]_2O_2(OH)_2$. A phase with such a composition has not been found in Nature yet.

Based on the *empirical data* known to date, the *simplified formula* of betalomonosovite can be written as $Na_{5+x}Ti_4[Si_2O_7]_2[PO_3(OH)]_{2-y}[PO_2(OH)_2]_yO_2[(OH,F)_{2-z}O_z]$, where $0 \le x \le 2$, $0 \le y \le 1$ and $0 \le z \le 1$. However this formula is quite simplified and describes only incompletely the chemical variability and crystal-chemical complexity of this mineral, especially in the interlayer content. Phosphate groups require special attention because the $PO_3(OH)$ group in the suggested formula *reflects the degree of protonation* only, but not the type of H-bearing groups. In fact, the presence of either $PO_3(OH)$ or $PO_2(OH)_2$ groups or even both of them is possible (Table 10). In all studies on the crystal chemistry of betalomonosovite, except for Rastsvetaeva *et al.* (1975) and Khalilov (1990), the interlayer content is not charge balanced (Table 1). Besides, the simplified formula $Na_6Ti_4[Si_2O_7]_2[PO_2(OH)_2]_2O_2(OH,F)_2$ suggested by Khalilov (1990) has an excess charge of +2. Rastsvetaeva (1986, 1988) did not provide ideal formula(e) of betalomonosovite but, in the crystal-chemical formulae, substitutions in several cation sites were introduced for charge balance without any substitutions in the anion sites of the *HOH* block. Khalilov (1990) and Sokolova *et al.* (2015a) introduced the substitution of O^{2-} by a univalent anion (OH^- or F^-) at the Ti–O–Ti bridges in the *O* sheet for the charge balance without losing Na in the *HOH* block. Yakubovich *et al.* (2014) introduced both mechanisms in the crystal-chemical formula, but did not give an idealized (simplified) formula. This contradicts the local charge balance and put the reported models in doubt. Thus there is no evidence for the presence of only doubly protonated phosphate groups $[PO_2(OH)_2]$ in the samples of betalomonosovite reported to date.

Besides, the simplified formula $Na_6\square_4Ti_4(Si_2O_7)_2[PO_3(OH)][PO_2(OH)_2]O_2(OF)$ suggested by Sokolova *et al.* (2015a) contains species-defining fluorine, despite the fact that this constituent is very uncommon for lomonosovite (see Lykova (2015) and references therein) and is rare for betalomonosovite, as shown by our sampling. Indeed, F^- occasionally replaces O^{2-} at the Ti–O–Ti bridge as a result of post-crystallization transformation of lomonosovite. It plays the same charge-balancing role as OH^- but typically occurs in minor amounts, and therefore should be considered in the general case as a subordinate admixture: (OH,F). Moreover, the F content in the original

holotype betalomonosovite is below the detection limit (Gerasimovskiy & Kazakova, 1962). Thus, the idealized formula of betalomonosovite should be F-free.

7. Conclusions

Betalomonosovite is a heterophyllosilicate mineral structurally closely related to lomonosovite, $Na_{10}Ti_4(Si_2O_7)_2(PO_4)_2O_4$. Distinctive features of betalomonosovite in comparison to lomonosovite are: (a) the invariable presence of H^+ in the form of species-defining acid phosphate anion(s) $[PO_2(OH)_2] \pm [PO_3(OH)]$ with the same content of phosphorus, 2P *apfu*; (b) the presence of OH^- ($\pm F^-$) substituting O^{2-} at the Ti–O–Ti bridges in the *O* sheet of the *HOH* heteropolyhedral block; (c) the associated deficiency of Na. Betalomonosovite demonstrates significant chemical and structural variability. Variations of the Na content, ratios of different phosphate anions and the degree of protonation of O atoms at the Ti–O–Ti bridges in the *O* sheet result in structural variations including different arrangements of PO_4 tetrahedra (provoking two types of unit cell, lomonosovite-like and with the doubled *b* parameter) and different occupancies of Na sites. Thus, this mineral is represented by several varieties; this phenomenon is definitely the main reason for the discrepancies between the structure data reported by Rastsvetaeva *et al.* (1975), Rastsvetaeva (1986, 1988, 1989), Khalilov (1990), Yakubovich *et al.* (2014) and Sokolova *et al.* (2015a). The simplified formula of betalomonosovite can be written as $Na_{5+x}Ti_4[Si_2O_7]_2[PO_3(OH)]_{2-y}[PO_2(OH)_2]_yO_2[(OH,F)_{2-z}O_z]$, where $0 \le x \le 2$, $0 \le y \le 1$ and $0 \le z \le 1$.

Our data show that betalomonosovite is a transformation mineral species [in terminology suggested by Khomyakov (1995)]: we believe that it cannot crystallize directly from a melt or solution. It forms at the expense of lomonosovite due to the leaching of Na and protonation of the O atoms in phosphate groups and at the Ti–O–Ti bridges in the *O* sheet without losing phosphorous. A hypothetic final product of lomonosovite alteration with preservation of 2P *apfu* seems corresponding to the H-richest and Na-lowest variety of betalomonosovite with the simplified formula $Na_4Ti_4[Si_2O_7]_2[PO_2(OH)_2]_2O_2(OH)_2$, but such a phase has not been found in Nature yet. The mechanisms and the degree of lomonosovite alteration to form betalomonosovite may vary significantly.

Thus the post-crystallization alteration of the primary high-temperature H-free mineral lomonosovite, $Na_{10}Ti_4(Si_2O_7)_2(PO_4)_2O_4$, can follow two essentially different pathways leading to the formation of minerals quite different in nature of H-bearing groups: (1) acid phosphate anion(s) $[PO_2(OH)_2] \pm [PO_3(OH)]$ with the formation of betalomonosovite, $Na_{5+x}Ti_4[Si_2O_7]_2[PO_3(OH)]_{2-y}[PO_2(OH)_2]_yO_2[(OH,F)_{2-z}O_z]$ with $0 \le x \le 2$, $0 \le y \le 1$ and $0 \le z \le 1$, or (2) H_2O molecules resulting in its transformation to murmanite, $Na_4Ti_4(Si_2O_7)_2O_4 \cdot 4H_2O$ (Borneman-Starynkevich, 1946; Ageeva, 1999; our data). The further transformation of betalomonosovite to murmanite is also possible (Lykova *et al.* 2016). However, the exact conditions of these transformation are still not completely clear and need further laboratory experiments and natural observations.

Acknowledgements: We are grateful to V.V. Borisova and A.V. Voloshin for their help in the providing of the GIM6019 specimen of betalomonosovite. We thank Péter Németh and Sergey Aksenov for their valuable comments and Sergey V. Krivovichev and Christian Chopin for their editorial work. The studies of crystal structure of betalomonosovite, its comparative crystal chemistry and mechanisms of formation were supported by the Russian Science Foundation, grant no. 14-17-00048. Special thanks are due to S.V. Fedyushchenko for the support of researches of ISL.

References

Ageeva, O.A. (1999): Typomorphism of accessory lomonosovite from rocks of the Khibiny massif. *Zap. Vseross. Mineral. Obs.*, **128**, 99–104 (in Russian).

Belov, N.V., Gavrilova, G.S., Solov'eva, L.P., Khalilov, A.D. (1977): The refined structure of lomonosovite. *Sov. Phys. Dokl.*, **235**, 1064–1067 (in Russian).

Borneman-Starynkevich, I.D. (1946): On chemical nature of murmanite. in "Problems of Mineralogy, Geochemistry and Petrography", D.S. Belyankin, ed. AN USSR, Moscow-Leningrad, 66–74 (in Russian).

Borutzky, B.E., Ageeva, O.A., Karimova, O.V., Kartashov, P.M., Yakubovich, O.V. (2014): New data on betalomonosovite. *New Data Miner.*, **49**, 23–41.

Brese, N.E. & O'Keeffe, N.E. (1991): Bond-valence parameters for solids. *Acta Crystallogr.*, **47**, 192–197.

Cámara, F., Sokolova, E., Hawthorne, F.C., Abdu, Y. (2008): From structure topology to chemical composition. IX. Titanium silicates: revision of the crystal chemistry of lomonosovite and murmanite, Group-IV minerals. *Mineral. Mag.*, **72**, 1207–1228.

Chukanov, N.V. (2014): Infrared Spectra of Mineral Species: Extended Library. Springer-Verlag, Dordrecht, 1716 p.

Chukanov, N.V. & Chervonnyi, A.D. (2016): Infrared Spectroscopy of Minerals and Related Compounds. Springer Verlag, Cham, 1109 p.

Ferraris, G. & Gula, A. (2005): Polysomatic aspects of microporous minerals – heterophyllosilicates, palysepioles and rhodesite-related structures. *Rev. Mineral. Geochem.*, **57**, 69–104.

Gerasimovskiy, V.I. & Kazakova, M.E. (1962): Betalomonosovite. *Dokl. Akad. Nauk SSSR*, **142**, 118–121 (in Russian).

Khalilov, A.D. (1990): Refinement of crystal structure of betalomonosovite from the Lovozero alkaline massif. *Mineral. Zhurnal*, **12**, 10–18 (in Russian).

Khomyakov, A.P. (1995) Mineralogy of Hyperagpaitic Alkaline Rocks. Clarendon Press, Oxford, 223 p.

Libowitzky, E. (1999): Correlation of O–H stretching frequencies and O–H···O hydrogen bond lengths in minerals. *Monatsh. Chem.*, **130**, 1047–1059.

Lykova, I.S. (2015): Minerals of the Epistolite Group: postcrystallization transformations and their crystal chemical mechanisms (natural systems and modelling experiments). PhD thesis, Lomonosov Moscow State University (in Russian).

Lykova, I.S., Pekov, I.V., Zubkova, N.V., Chukanov, N.V., Yapaskurt, V.O., Chervonnaya, N.A., Zolotarev Jr., A.A. (2015): Crystal chemistry of cation-exchanged forms of epistolite-group minerals. Part I. Ag- and Cu-exchanged lomonosovite and Ag-exchanged murmanite. *Eur. J. Mineral.*, **27**, 535–549.

Lykova, I.S., Pekov, I.V., Chukanov, N.V., Belakovskiy, D.I., Yapaskurt, V.O., Zubkova, N.V., Britvin, S.N., Giester, G. (2016): Calciomurmanite, $(Na,\square)_2Ca(Ti,Mg,Nb)_4[Si_2O_7]_2O_2(OH,O)_2(H_2O)_4$, a new mineral from the Lovozero and Khibiny alkaline complexes, Kola Peninsula, Russia. *Eur. J. Mineral.*, **28**, 835–845.

Moiseev, M.M. & Chukanov, N.V. (2007): Mineralogy of Alkaline Pegmatites and Hydrothermalites of the Kovdor Phlogopite Deposit. *New Data Miner.*, **41**, 46–55.

Nakamoto, K. (2008): Infrared and Raman Spectra of Inorganic and Coordination Compounds, Theory and Applications in Inorganic Chemistry. John Wiley and Sons, New York, 350 p.

— (2009): Infrared and Raman Spectra of Inorganic and Coordination Compounds, Part B, Applications in Coordination, Organometallic, and Bioinorganic Chemistry. John Wiley and Sons, Hoboken, 424 p.

Pekov, I.V. (2000): Lovozero Massif: History, Pegmatites, Minerals. Ocean Pictures Ltd., Moscow, 480 p.

Rastsvetaeva, R.K. (1986): Crystal structure of betalomonosovite from the Lovozero region. *Sov. Phys. Crystallogr.*, **31**, 633–636.

— (1988): Crystal structure of the disordered modification of betalomonosovite. *Zap. Vses. Mineral. Obs.*, **117**, 696–705 (in Russian).

— (1989): On structure transformations in betalomonosovite. *Kristallografiya*, **34**, 880–884 (in Russian).

Rastsvetaeva, R.K., Sirota, M.I., Belov, N.V. (1975): Crystal structure of betalomonosovite. *Sov. Phys. Crystallogr.*, **20**, 158–160.

Sheldrick, G.M. (2008): A short history of SHELX. *Acta Crystallogr.*, **A64**, 112–122.

Sokolova, E. (2006): From structure topology to chemical composition. I. Structural hierarchy and stereochemistry in titanium disilicate minerals. *Can. Mineral.*, **44**, 1273–1330.

Sokolova, E., Abdu, Y., Hawthorne, F.C., Genovese, A., Cámara, F., Khomyakov, A.P. (2015a): From structure topology to chemical composition. XVIII. Titanium silicates: revision of the crystal structure and chemical formula of betalomonosovite, a group-IV TS-block mineral from the Lovozero alkaline massif, Kola Peninsula, Russia. *Can. Mineral.*, **53**, 401–428.

Sokolova, E., Hawthorne, F.C., Abdu, Y.A., Genovese, A., Cámara, F. (2015b): Reapproval of betalomonosovite as a valid mineral species: single-crystal X-ray diffraction, HRTEM, Raman and IR. *Periodico di Mineralogia*, ECMS2015, 157–158.

Sokolova, M.N., Zabavnikova, N.I., Rudnitskaya, E.S., Yakovlevskya, T.A. (1971): Betalomonosovite from the Khibiny massif. *Izv. Akad. Nauk SSSR, Ser. Geol.*, **2**, 77–84 (in Russian).

Yakubovich, O.V., Karimova, O.V., Ageeva, O.A., Borutzky, B.E. (2014): Crystal structure of betalomonosovite: new data. *Zap. Vseross. Mineral. Obs.*, **143**, 88–103 (in Russian).

Received 24 January 2017
Modified version received 10 May 2017
Accepted 7 September 2017